IEEE Access
Multidisciplinary ⋮ Rapid Review ⋮ Open Access Journal

Received April 10, 2020, accepted May 3, 2020, date of current version June 4, 2020.

Digital Object Identifier 10.1109/ACCESS.2020.2994374

A Novel Force Sensorless Reflecting Control for Bilateral Haptic Teleoperation System

CONG PHAT VO[1], XUAN DINH TO[1,2], AND KYOUNG KWAN AHN[1], (Senior Member, IEEE)
[1]School of Mechanical and Automotive Engineering, University of Ulsan, Ulsan 44610, South Korea
[2]Faculty of Control Engineering, Le Quy Don Technical University, Hanoi 100000, Vietnam

Corresponding author: Kyoung Kwan Ahn (kkahn@ulsan.ac.kr)

This work was supported by the Basic Science Research Program through the National Research Foundation of Korea (NRF) funded by the Ministry of Science and ICT, South Korea under Grant NRF-2020R1A2B5B03001480.

ABSTRACT This paper presents a novel force sensorless reflecting controller for a haptic-enabled device driven by a bilateral pneumatic artificial muscle system, which proposed configuration for the first time the bilateral haptic teleoperation. For details, an adaptive force observer scheme considered to be an alternative to direct force measurement is proposed to estimate the interaction force with an unknown environment for the force reflecting control design. Meanwhile, the separately fast finite time nonsingular terminal sliding mode control schemes are developed based on the force estimation in both subsystems to achieve good tracking performance and fast response. Thus, the great transparency performance with both force feedback and position tracking can be achieved simultaneously by using our proposed method. The finite-time stability of the total controlled system is demonstrated by the Lyapunov approach. Moreover, the comparative experiments are carried out on the developed testbench to validate the effectiveness and advantages of our proposed control design in the different working conditions.

INDEX TERMS Bilateral teleoperation system, pneumatic muscle actuator, force observer.

I. INTRODUCTION

In recent years, the teleoperation techniques have been developed to reach a high level of sophistication and rapidly played an important role in numerous practical applications, such as robotic surgery, nuclear source detection, robotic construction [1]–[4]. Besides, these systems required the possibility of physical interaction with the remote environment to provide the feeling of the present there, called haptic. From a design perspective, many actuators are employed in the haptic teleoperation systems to supply sensory feedback. Specifically, motor-driven actuators [5] are widely used given their characteristics of safety and capability of providing suitable force for small haptic devices according to the required state. However, they are incompatible with the applications that have extensively magnetic interference because of producing their own magnetic fields. Meanwhile, the pneumatic artificial muscle actuators (PAMs) possessed the advantages of a lightweight, reasonable safety and a high power-to-weight ratio, which have been considered as one of the most promising solutions for haptic devices in many applications such as robot-assisted surgery, rescue robots, etc [3], [6], [7]. In this work, a bilateral haptic teleoperation system actuated by a pair of antagonistic PAM (APAM) configuration was first designed.

The teleoperation system can be called a bilateral system as the human not only operates the master system and transmits the command trajectories to the slave system and interacts with an environment but the interaction signals between the slave and the environment can also be feedbacked to the human through the master. Both master and slave robots are controlled bilaterally with the same actions of force and motion movements. The bilateral teleoperation hereby is normally assessed through two critical indices of stability and transparency. To be more specific, stability requires the closed-loop system to be stable under different environmental conditions. Transparency presents how well the haptic feedback cues provide the human operator slave-environment interaction. Numerous control strategies have been introduced to balance the trade-off between these indices [7], [8]. Besides, much effort has been made to seek robust control methods to obtain satisfactory control performance. For example, based on the system model [9], the conventional Proportional-Integral-Derivative (PID) controller

The associate editor coordinating the review of this manuscript and approving it for publication was Xiwang Dong.

for a robotic arm was designed. An advanced PID controller combined with a neural network scheme [7] and an intelligent phase plane switching controller [10]. However, the above approaches are only efficient in several specific regions without high nonlinearity and time variation of system parameters. To improve these restrictions, a variety of advanced methods was proposed such as a fuzzy approach [11], [12], a neural network [13], a time-delay-based control [14], [15] and radial basis function neural network [16]. Nonetheless, the above approaches require complicated algorithms or a large number of tuning parameters and depend largely on the experience of experts. It is worth noting that sliding mode control (SMC) is one of the most powerful methods to enhance the nonlinear systems with uncertainties and disturbances [17], [18]; however, the SMC can only asymptotically achieve stability for the controlled system. Taking advantage of SMC, the terminal SMC (TSMC) has been developed with its superiorities such as finite-time convergence and high tracking accuracy [19]–[23]. Successively, the modified version of TSMC namely the fast nonsingular TSMC (FNTSMC) is developed to not only guarantee fast convergence rate in the sliding phase when the system states are far away from the equilibrium [24], but also avoiding a singularity of switching from terminal sliding surface to linear sliding surface [25]. From a haptic control perspective, the APAM actuated haptic device is a challenge since its dynamic contains high uncertainties.

Additionally, the transparency of a bilateral teleoperation system requires not only accurate master-slave position tracking but also exact force perception. Thus, force information is a crucial element to enhance the robotic system performance with a force reflecting control scheme [26]. The force sensing technique plays a vital role in such force control designs since the control performance is affected by the precision of the force detection. In conventional approaches, the force information is obtained from force sensors. However, the usage of force sensors is not always available or feasible in practical applications owing to some drawbacks such as high cost, inconvenience to install, the capability of being damaged by collisions and narrow bandwidth due to their sensitivity to large noise [27], [28]. Therefore, the force information can be obtained by force observers and have been proposed in many approaches [29]–[33]. In [33], a nonlinear disturbance observer (NDOB) is a well-known estimation method for estimating the external force signal of the bilateral teleoperation system. In another approach presented in [34], an extend active observer (EAOB) estimated both force and state information to improve control performance by removing the effect of measurement noise and parametric uncertainties. An extended state observer with an adaptive gain was also designed to obtain the force and state information without using force sensors in the bilateral teleoperation system in [27]. Even though these observers provide a simple way to estimate the external force, their disadvantage is the effects of noise as the velocity computation could deteriorate the force sensing. To handle this issue, the combination of force observer with a Kalman filter was introduced in [35], [36]. However, the Kalman filter cannot guarantee the finite-time convergence of the estimation errors, which could lead to difficulty in ensuring global control stability. With the wish to develop the simple, fast and robust online estimation, the novel adaptive force observer (AFOB) is proposed to estimate external forces without using any load cell. It is worth noting that the globally exponential stability still guarantees the good performance of the bilateral teleoperation system. That results are used to design robust controllers for the bilateral teleoperation in the presence of parameter uncertainties.

According to the above analysis, this paper proposes control schemes based on a combination of AFOB and FNTSMC scheme in a manipulated smart deburring regardless of a dynamic model and parametric uncertainties for the master and slave systems, which can guarantee the stability with fast convergence error and tight tracking performance. Motivated by the preceding discussions, as well as shortcomings in the existing literature, the main originalities of this paper can be summarized as follows.

- From our knowledge, there are no studies for the bilateral haptic teleoperation based on the APAM configuration. Moreover, this work proposed for the first time the hybrid control based on a fast finite-time NTSMC and AFOB. The objective of this work is to investigate the interesting above-mentioned properties of the proposed approach.
- The stability and finite-time convergence characteristic of the closed-loop control are theoretically analyzed by the Lyapunov approach.
- The experimental results are conducted on a designed PAM actuated haptic system and the effectiveness of the proposed control method is verified in the different working conditions.

The remains of this paper are organized as follows. The force dynamic model of the PAM system is presented in Section 2. In Section 3, the adaptive force observer scheme, the haptic control based FNTSMC and the stability analysis of the controlled system are investigated. The experimental results are carried out in Section 4. Finally, concluding remarks and future works are given in Section 5.

II. FORCE DYNAMICS OF THE APAM SYSTEM

In this research, the master-slave robots with a single degree of freedom were configurated to create a sense of touch. The concept of bilateral control is proposed on the basis of the exchanged information between the master robot and the slave robot. The master robot provides an operator human-machine interface to feel force feedback, which relied on imposing to the control stick through the pair of APAM configuration. On the other hand, a slave robot is applied to interact with unknown environments.

For determining the nonlinear model of the PAM, the theoretical models of the PAMs were presented in [37] which described the major characteristics of the PAM are the relation between pressure, force, volume, and length. Besides,

the phenomenological models of PAMs were investigated in [38], [39] which express the output force as a function of pneumatics' pressure and kinematics. In this study, the three-element phenomenological model considering the hysteresis phenomenon presented in [39] is adopted to describe the dynamics of the PAM. The expression of the approximated force exerted by a single PAM based on its pressure and contraction strain follows the constitutive laws.

$$M_k\ddot{\xi}_k + b_k(P_k)\dot{\xi}_k + k_k(P_k)\xi_k = f_k(P_k)$$
$$\begin{cases} b_k(P_k) = b_{k1}P_k + b_{k0} \\ k_k(P_k) = k_{k1}P_k + k_{k0} \\ f_k(P_k) = f_{k1}P_k + f_{k0} \end{cases} \quad (k = 1, 2) \tag{1}$$

where M_k, ξ_k, P_k are the mass of load, the displacement and air pressure of the k^{th} PAM, respectively; $b_k(P_k)$, $k_k(P_k)$, and $f_k(P_k)$ are the damping coefficient, stiffness, and the contraction force of the k^{th} PAM, respectively; b_{k1}, b_{k0}, k_{k1}, k_{k0}, f_{k1}, and f_{k0} are the coefficients of the model parameters.

In fact, two proportional valves integrated inside the pressure regulators were used to regulate the pressure of the compressed air supplied into the PAMs. Consequently, the position is obtained through the antagonistic control of the pressure of the pair of the PAMs. A positive/negative motion of the plate requires an increment/decrement of the pressure P_1 of the PAM 1 and a decrement/increment of the pressure P_2 of the PAM 2. Therefore, the antagonistic actuation can be described by:

$$P_1 = P_0 + \Delta P, \quad P_2 = P_0 - \Delta P \tag{2}$$

where $P_0 = 3$ bar is the initial pressure and ΔP is the pressure difference from P_0 used as a manipulated variable in the antagonistic pressure control. In the APAM system, the two PAMs are connected by a rod and through a pulley with a radius of $r = 0.025$ m. Given two contraction forces, one from each muscle, the torque τ of the actuated joint reads

$$\tau = \tau_1 - \tau_2 = r(f_1 - f_2) \tag{3}$$

where τ_1 and τ_2 are the torques generated by each PAM.

The total torque can be expressed in terms of the joint angle θ, using the kinematic relations

$$\theta = (\xi_1 - \xi_2)/r \tag{4}$$

Hence, the dynamic of the robot can be written as the following nonlinear second-order equation.

$$M\ddot{\theta} + C\dot{\theta} + K\theta = \tau - \tau_d \tag{5}$$

where $M = M_k r^2$, $C = (\zeta + 2r^2(b_{11}P_0 + b_{10}))$, $K = 2r^2(k_{11}P_0 + k_{10}))$, $\zeta = 0.052$ N.s/m is the viscous damping coefficient, τ_d is the total of unknown disturbances in the system dynamics, which includes of external perturbations, e.g., load variations or disturbance torque, and friction nonlinearities and M_k denotes the link inertia which is estimated of inertia amounts to 0.032 kg.m^2. This value can be obtained from the CAD 3D model of the robot after specifying the materials of the parts of the model. The specification parameters of the APAM model are given in Table 1. Fig. 1 expresses the open loop responses of the model and the real APAM system with respect to a chirp control input signal of the frequency of 0.01 Hz and the reducing amplitude by the function $4\pi \times (1 - 0.03t)$ via sampling time t. As can be seen in this figure, the dynamics model described in (5) can fairly represent the high nonlinearity of the real system with small estimation error. The dynamic model of 1 DOF master and slave system based on APAM for the haptic system is given as follows

$$M_m\ddot{\theta}_m + C_m\dot{\theta}_m + K_m\theta_m = \tau_m - \tau_{md} \tag{6}$$
$$M_s\ddot{\theta}_s + C_s\dot{\theta}_s + K_s\theta_s = \tau_s - \tau_{sd} \tag{7}$$

where m and s denote the master and slave side, respectively. Let i denotes m or s, in (6) and (7). $\theta_i(t)$, $\dot{\theta}_i(t)$, $\ddot{\theta}_i(t)$, represents the joint position, velocity and acceleration,respectively. $\tau_i(t)$is the applied control torque and $\tau_{id}(t)$ denotes the external torque, for $i = m,s$. According to [41], one of the fundamental properties of the bilateral teleoperation systems (6) and (7), matrices $\dot{M}_i - 2C_i$ are skew-symmetric.

TABLE 1. List of APAM model parameters.

	Parameter	Value	Units
Spring elements	k_{k1}	117.32	N/m/bar
	k_{k0}	6.8	N/m
Damping elements	b_{k1}	96.2	N/m/s/bar
	b_{k0}	0.85	N/m/s
Force elements	f_{k1}	91.22	N/bar
	f_{k0}	4.73	N

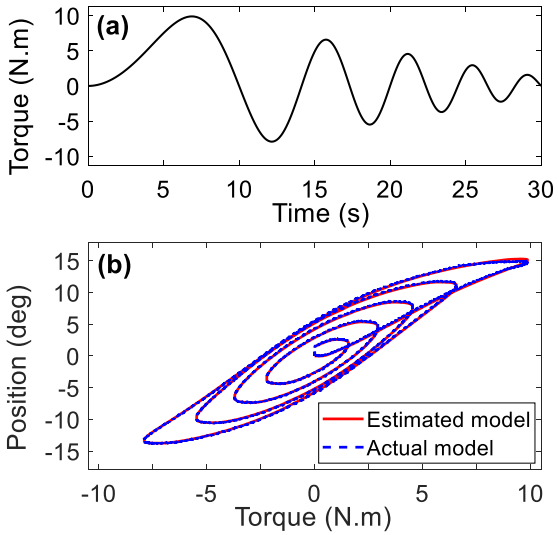

FIGURE 1. Response of the APAM system. (a) The chirp control signal, (b) Hyteresis curve.

III. THE NONLINEAR BILATERAL CONTROLLER DESIGN

In this section, the bilateral control of force and motion in the PAM based haptic system is presented. The concept of bilateral control is introduced on the basis of the exchanged information between the master side and the slave side.

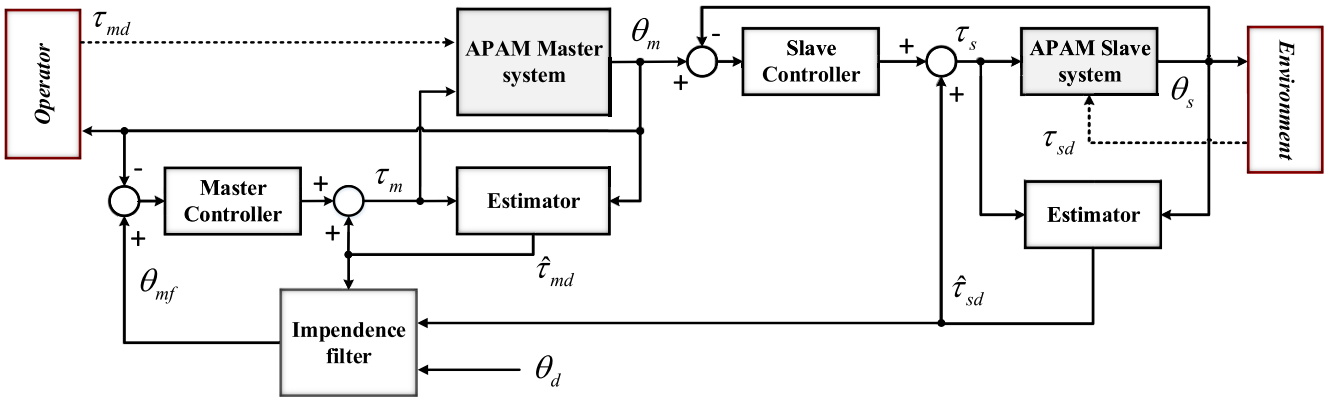

FIGURE 2. Proposed bilateral control scheme for APAM actuated haptic system.

The force sensing to the human operator is supplied through the master system. Meanwhile, the slave system is employed to interact with environments. The bilateral control design for the overall haptic system can be achieved the globally stable of the closed-loop system. Particularly, the PAM based slave system θ_s can track the desired trajectory of the master side θ_m with guarantee the error as small as possible. Consequently, the great transparency is demonstrated through a good impedance performance of the master system so that the human can have the actual feeling of the contact force with the environment vividly when the system is in a steady state.

To start with, the proposed control algorithm of a bilateral haptic teleoperation system is shown in Fig. 2. The operator applied torque and the environment torque is approximated using the proposed adaptive force observers. Then, the estimated contact force $\hat{\tau}_{sd}$ is transmitted to the master subsystem. Through the impedance filter block, the desired trajectory of the master system is derived to attain the desired impedance performance and provide good force feedback performance for the operator. The fast nonsingular terminal sliding mode scheme is designed separately for the master system to drive the master position to track the generated reference trajectory as fast and accurately as possible. The master output position θ_m is then sent back to the slave system and becomes the reference for the slave-side position tracking control. The robust control scheme is designed for the slave system to achieve great tracking performance in the presence of uncertainties and nonlinearities. Subsequently, the global stability of the overall system and good transparency performance including position tracking and force feedback is simultaneously achieved.

A. CONTACT FORCE ESTIMATION USING ADAPTIVE OBSERVER

In this section, a novel AFOB approach is designed to estimate the force information for the system without the adoption of a force sensor. The force information is employed for a force reflecting control scheme in the next section. Firstly, the following auxiliary variables are defined:

$$x_{1i} = \theta_i, x_{2i} = \dot{\theta}_i, \tag{8}$$

As found in [40], the nominal system of (6) and (7) is represented by the following form

$$\dot{x}_{2i} = \Lambda_i - \bar{M}_i^{-1}\bar{\Delta}_i + \sigma_i\tau_{id} \tag{9}$$

where $\sigma_i = -\bar{M}_i^{-1}$, $\Lambda_i = \bar{M}_i^{-1}(\tau_i - \bar{C}_i x_{2i} - \bar{K}_i x_1)$ with $\bar{M}_i, \bar{C}_i, \bar{K}_i$ are the nominal values of the inertia term M_i, damping term C_i, stiffness term K_i, respectively; $\bar{\Delta}_i$ is the total of unknown disturbance and modeling errors;

Assumption 1: The norm of $\bar{\Delta}_i$ is bounded by the following inequation.

$$\left\|\bar{\Delta}_i\right\| \leq \bar{\omega}_i, \tag{10}$$

where $\bar{\omega}_i$ is a positive constant.

Let the filtered variable σ_i^*, Λ_i^* and x_{2i}^* as

$$\begin{cases} m\dot{\sigma}_i^* + \sigma_i^* = \sigma_i, & \sigma_i^*(0) = 0 \\ m\dot{\Lambda}_i^* + \Lambda_i^* = \Lambda_i, & \Lambda_i^*(0) = 0 \\ m\dot{x}_{2i}^* + x_{2i}^* = x_{2i}, & x_{2i}^*(0) = 0 \end{cases} \tag{11}$$

where m is a positive value. Ideally, an invariant manifold is then raised to design an unknown input observer.

The following auxiliary variables are defined.

$$\vartheta = \frac{(x_{2i} - x_{2i}^*)}{m} - \Lambda_i^* - \sigma_i^*\tau_{id} \tag{12}$$

From (11) and (12), the time derivative of ϑ is obtained as

$$\begin{aligned} \dot{\vartheta} &= -\frac{1}{m}\left(\frac{x_{2i} - x_{2i}^*}{m} - \Lambda_i^* - \sigma_i^*\tau_{id}\right) - \frac{\bar{M}_i^{-1}\bar{\Delta}_i}{m} - \sigma_i^*\dot{\tau}_{id} \\ &= -\frac{1}{m}\left(\vartheta + \bar{M}_i^{-1}\bar{\Delta}_i + m\sigma_i^*\dot{\tau}_{id}\right). \end{aligned} \tag{13}$$

Lemma 1: Consider the system (9) with the filter (11), the variable ϑ is ultimately bounded for any finite a positive value of m and decreases in an exponential sense. Additionally, the manifold $\lim_{a\to 0}(\lim_{t\to\infty}[\vartheta]) = 0$ is invariant for $m \to 0$.

Proof: The proof of the lemma is shown in Appendix A.

According to the swapping lemma in [42] and applying a filter $1/(ms+1)$ on both sides of (11) for any finite $m > 0$, we have:

$$\frac{1}{m}(x_{2i} - x_{2i}^*) = \Lambda_i^* + \sigma_i^* \tau_{id} + \frac{m}{ms+1}\sigma_i^* \dot{\tau}_{id} + \frac{1}{ms+1}\bar{M}_i^{-1}\bar{\Delta}_i \tag{14}$$

where the last two terms $\psi = [m/(ms+1)][\sigma_i^* \dot{\tau}_{id}] + [1/(ms+1)][\bar{M}_i^{-1}\bar{\Delta}_i]$ from the filtering external torques of $[\sigma_i^* \dot{\tau}_{id}]$ and the uncertainties $\bar{M}_i^{-1}\bar{\Delta}_i$. If τ_{id} is constant and $\bar{\Delta}_i = 0$, then $\psi = 0$. Since σ_i is bounded, its filtered function σ_i^* is also bounded, i.e., $\|\sigma_i^*\| \leq \mu_\sigma$ for a constant μ_σ. As the external torques τ_{id} and its derivative is bounded, ψ is bounded for any finite a positive value of m, i.e., $\|\psi\| \leq \bar{\psi}$. In this case, ψ can be regarded as disturbances unsettling the ideal manifold $\Phi = 0$ in Lemma 1.

Considering the approach as in [43], [44], the variables of the proposed adaptive law are defined as

$$\begin{cases} \Gamma_1 = \Upsilon_1 \hat{\tau}_{id} - \Upsilon_2 \\ \Gamma_2 = \sigma_i^{*T}\sigma_i^* \hat{\tau}_{id} - \sigma_i^{*T}((x_{2i} - x_{2i}^*)/m - \Lambda_i^*) \end{cases} \tag{15}$$

where $\hat{\tau}_{id}$ is the estimate of τ_{id}, $\dot{\Upsilon}_1 = -a\Upsilon_1 + \sigma_i^{*T}\sigma_i^*$, and $\dot{\Upsilon}_2 = -a\Upsilon_2 + \sigma_i^{*T}((x_{2i} - x_{2i}^*)/m - \Lambda_i^*)$ when $\Upsilon_1(0) = 0$ and $\Upsilon_2(0) = 0$, respectively, with a is a positive constant scalar.

Lemma 2: The variables in (15) are equivalent to

$$\begin{cases} \Gamma_1 = -\Upsilon_1 \tilde{\tau}_{id} + \Omega \\ \Gamma_2 = -\sigma_i^{*T}\sigma_i^* \tilde{\tau}_{id} + \sigma_i^* \psi \end{cases} \tag{16}$$

where $\Omega = \int_0^t e^{-a(t-\tau)}\sigma_i^{*T}(\tau)(\sigma_i^*(\tau)(\tau_{id}(t) - \tau_{id}(\tau)) + \psi(\tau))d\tau$ is a bounded residual error satisfying $\|\Omega\| \leq (2\mu_\sigma^2 \varepsilon_{\tau_i} + \mu_\sigma \bar{\psi})/a$, with $\tilde{\tau}_{id} = \tau_{id} - \hat{\tau}_{id}$ are the estimation errors and $\|\tau_{id}\| \leq \varepsilon_{\tau_i}$.

Proof: The proof of the lemma is shown in Appendix B.

An adaptive gain κ is calculated as

$$\dot{\kappa} = a\kappa - \kappa \sigma_i^{*T}\sigma_i \kappa \tag{17}$$

Then, taking the integral (17), which can be obtained as follows

$$\begin{aligned} \kappa^{-1} &= e^{-at}\kappa_0 + \int_0^t e^{-a(t-\tau)}\sigma_i^{*T}(\tau)\sigma_i^*(\tau)d\tau \\ &= e^{-at}\kappa_0 + \Upsilon_1 \end{aligned} \tag{18}$$

where the fact that $(d/dt)\kappa\kappa^{-1} = \dot{\kappa}\kappa^{-1} + \kappa(d/dt)\kappa^{-1} = 0$.

From (18) discloses that κ converges to the inverse of Υ_1. In [45], the definition of the persistently exciting, i.e., $\int_t^{t+T}\sigma^T(\tau)\sigma(\tau)d\tau \geq \beta$ for any finite t, T, β are positive values. Since $\int_0^t e^{-a(t-\tau)}\sigma^T(\tau)\sigma(\tau)d\tau > \int_{t-T}^t e^{-aT}\sigma^T(\tau)\sigma(\tau)d\tau \geq \beta e^{-aT}$ holds for $t > T$. Hence, $\lambda_{\min}(\Upsilon_1) > \beta e^{-aT} > 0$ holds that $\Upsilon_1 > \beta e^{-aT} > 0$. Thus,

$$\kappa^{-1}(t) \leq \kappa^{-1}(0) + \mu_\sigma^2 \int_0^t e^{-a(t-\tau)}d\tau \leq \kappa_0 + \mu_\sigma^2/a. \tag{19}$$

From (19) the boundedness of κ can be derived as

$$\kappa^{-1}(t) = e^{-at}\kappa(0) + \Upsilon_1(t) \geq e^{-aT}\beta. \tag{20}$$

Combination (19) and (20) show that

$$\left(\lambda_{\min}(\kappa_0) + \mu_\sigma^2/a\right)^{-1} \leq \kappa(t) \leq e^{aT}\beta^{-1}. \tag{21}$$

As a consequence, the adaptation law is expressed to estimate external torques as the following.

$$\dot{\hat{\tau}}_{id} = -\delta\kappa(\Gamma_1 + \eta\Gamma_2) \tag{22}$$

where δ, η is a positive scalar, and κ is the online updated value in (18).

Theorem 1: The boundedness of the external force estimation error $\|\tilde{\tau}_{id}\|$ is guaranteed the convergence to an expression defined by $\|\tilde{\tau}_{id}\| = \|\tau_{id} - \hat{\tau}_{id}\| \leq \bar{\zeta}_i$, where $\bar{\zeta}_i$ is a positive design parameter when σ is persistently exciting.

Proof: The proof of the theorem is shown in Appendix C.

B. MASTER CONTROL DESIGN

By measuring the active torque estimate applied by the operator, it is possible to compute the new reference trajectory required to make the master robot operate in certain mass, stiffness and damping parameters. As a result, the adapted angle θ_{mf} can be obtained with an impedance filter as follow:

$$\theta_{mf} = \frac{\hat{\tau}_{md} - \hat{\tau}_{sd}}{M_d s^2 + B_d s + K_d} + \theta_d \tag{23}$$

where M_d, B_d, K_d are the designed impendence parameters and θ_d is the initial desired command of the master subsystem.

In order hand to achieve good tracking performance and fast response of systems, a fast finite time nonsingular terminal sliding mode control is proposed for the master system in the presence. The tracking errors are defined as the following

$$\tilde{\theta}_m = \theta_{mf} - \theta_m, \dot{\tilde{\theta}}_m = \dot{\theta}_{mf} - \dot{\theta}_m \tag{24}$$

To obtain the terminal convergence of the tracking errors, a special variable called terminal sliding surface is designed as

$$s_m = \lambda_m \tilde{\theta}_m^{[\alpha_m]} + \dot{\tilde{\theta}}_m \tag{25}$$

where $\alpha_m = p_m/q_m$, p_m and q_m are positive odd integers satisfying $q_m > p_m$; λ_m is a positive parameter of the sliding surface.

From the system (6) and sliding surface formula (25), the derivative of the sliding surface with respect to time can be obtained as follows:

$$\begin{aligned} \bar{M}_m \dot{s}_m &= -\bar{M}_m \ddot{\tilde{\theta}}_{mf} + \bar{M}_m \lambda_m \alpha_m \tilde{\theta}_m^{[\alpha_m - 1]}\dot{\tilde{\theta}}_m \\ &\quad + \tau_m - \tau_{md} - \bar{C}_m \dot{\theta}_m - \bar{K}_m \theta_m \\ &= -\bar{M}_m \ddot{\tilde{\theta}}_{mr} - \bar{C}_m \dot{\tilde{\theta}}_{mr} - \bar{K}_m \theta_m + \tau_m - \tau_{md} - \bar{C}_m s_m \end{aligned} \tag{26}$$

where $\dot{\theta}_{mr} = s_m - \dot{\theta}_m = \dot{\theta}_{mf} + \lambda_m \tilde{\theta}_m^{[\alpha_m]}$. To preserve a fast finite-time convergence property, the reaching phase is chosen as follows:

$$s_m + \rho_{1m} s_m + \rho_{2m} s_m^{[\nu_m]} sign(s_m) = 0 \tag{27}$$

where ρ_{1m}, ρ_{2m} are the positive constants for the reaching phase and $0 < \nu_m < 1$.

By applying the haptic control based on force sensorless is embedded into the control system to simultaneously compensate for the effects caused by dynamic uncertainties. The control signal in the master side is introduced as follows:

$$\begin{aligned}\tau_m = {} & \bar{M}_m \ddot{\theta}_{mr} + \bar{C}_m \dot{\theta}_m + \bar{K}_m \theta_m \\ & - \varepsilon_m sign(s_m) - \rho_{1m} s_m - \rho_{2m} s_m^{[\nu_m]} + \hat{\tau}_{md}\end{aligned} \tag{28}$$

where ε_m is the bound value of the unexpected disturbances.

In the following, the sufficient condition for the stability of the master system is provided.

Theorem 2: For the master subsystem is presented in (6), with the bounded external force estimation in Theorem 1 and suppose that Assumption 1 is satisfied, i.e. $\varepsilon_m \geq \bar{\zeta}_m + \bar{\omega}_m$, if the sliding surface is designed as (25) and the control law is designed as (28), then the tracking error will converge to zero in a finite time.

Proof: The proof of the theorem is shown in Appendix D.

C. SLAVE CONTROL DESIGN

A reference trajectory is designed in the slave with the input of the master position signal θ_m, to produce the command trajectory for the tracking of the slave system.

The tracking errors are defined as the following

$$\theta_s = \theta_s - \theta_{sd}, \dot{\theta}_s = \dot{\theta}_s - \dot{\theta}_{sd} \tag{29}$$

where $\theta_{sd}(t)$ is the home position of the slave system. Then the sliding surfaces are designed as

$$s_s = \lambda_s \tilde{\theta}_s^{[\alpha_s]} + \dot{\tilde{\theta}}_s \tag{30}$$

where $\alpha_s = p_s/q_s$, p_s and q_s are positive odd integers satisfying $q_s > p_s$; λ_s is a positive parameter of the sliding surface.

Thus, the combination of the derivative of the sliding surface (30) with respect to time and the slave dynamic (7) can be obtained as follows:

$$\begin{aligned}\bar{M}_s \dot{s}_s &= -\bar{M}_s \ddot{\theta}_{sd} + \bar{M}_s \lambda_s \alpha_s \tilde{\theta}_s^{[\alpha_s - 1]} \dot{\tilde{\theta}}_s \\ &\quad + \tau_s - \tau_{sd} - \bar{C}_s \dot{\theta}_s - \bar{K}_s \theta_s \\ &= -\bar{M}_s \ddot{\theta}_{sr} - \bar{C}_s \dot{\tilde{\theta}}_{sr} - \bar{K}_s \theta_s + \tau_s - \tau_{sd} - \bar{C}_s s_s\end{aligned} \tag{31}$$

where $\dot{\theta}_{sr} = s_s - \dot{\theta}_s = \dot{\theta}_{sd} + \lambda_s \tilde{\theta}_s^{[\alpha_s]}$. Furthermore, in order to improve the convergence toward equilibrium zero, the reaching phase is chosen as follows:

$$s_s + \rho_{1s} s_s + \rho_{2s} s_s^{[\nu_s]} sign(s_s) = 0 \tag{32}$$

where ρ_{1s}, ρ_{2s} are the positive constants for the reaching phase and $0 < \nu_s < 1$. Thus, the slave controller can be designed as follows:

$$\begin{aligned}\tau_s = {} & \bar{M}_s \ddot{\theta}_{sr} + \bar{C}_s \dot{\theta}_s + \bar{K}_s \theta_s \\ & - \varepsilon_s sign(s_s) - \rho_{1s} s_s - \rho_{2s} s_s^{[\nu_s]} + \hat{\tau}_{sd}\end{aligned} \tag{33}$$

where ε_s is the bound value of the unexpected disturbances.

Theorem 3: For the slave system presented in (7) input of the master position signal θ_m with the bounded external force estimation in Theorem 1 and suppose that Assumption 1 is satisfied, i.e. $\varepsilon_s \geq \bar{\zeta}_s + \bar{\omega}_s$, if the sliding surface is designed as (30) and the control law is designed as (33), then the tracking error will converge to zero in a finite time.

Proof: The proof of the theorem is shown in Appendix E.

Furthermore, the i^{th} element (for $i = m, s$) of the surface s_i in (25) and (30) can be given as follows:

$$s_i = \lambda_i \tilde{\theta}_i^{[\alpha_i]} + \dot{\tilde{\theta}}_i \tag{34}$$

When the terminal sliding surface (34) is reached ($s_i = 0$), its derivative with respect to time is obtained as

$$\begin{aligned}\dot{s}_i &= \lambda_i \alpha_i \tilde{\theta}_i^{[\alpha_i - 1]} \dot{\tilde{\theta}}_i + \ddot{\tilde{\theta}}_i \\ &= -\lambda_i^2 \alpha_i \tilde{\theta}_i^{[2\alpha_i - 1]} + \ddot{\tilde{\theta}}_i\end{aligned} \tag{35}$$

It can be seen that, if $\alpha_i > 1/2$, then the singularity problem on the terminal sliding mode does not occur. Besides, in the case $\dot{\tilde{\theta}}_i \neq 0$ while $\tilde{\theta}_i = 0$ before the reaching phase $s_i \neq 0$, the modified terminal sliding surface is to deal with the singularity problem as the following [48]:

$$s_i = \Pi_i \left(\tilde{\theta}_i \right) + \dot{\tilde{\theta}}_i \tag{36}$$

where

$$\Pi_i(\tilde{\theta}_i) = \begin{cases} \lambda_i \tilde{\theta}_i^{[\alpha_i]}, & \text{if } s_i = 0 \text{ or } s_i \neq 0 \text{ and } \left|\tilde{\theta}_i\right| > \varsigma_i \\ z_{1i} \tilde{\theta}_i + z_{2i} \tilde{\theta}_i^2 sign(\tilde{\theta}_i), & \text{if } s_i \neq 0 \text{ and } \left|\tilde{\theta}_i\right| \leq \varsigma_i \end{cases}$$

with $z_{1i} = (2 - \alpha_i) \varsigma_i^{[\alpha_i - 1]}$, $z_{2i} = (\alpha_i - 1) \varsigma_i^{[\alpha_i - 2]}$, ς_i is a positive constant.

Remark 1: The range of the parameter α_i is defined as $1/2 < \alpha_i < 1$ to avoid the singularity problem.

Remark 2: According to the finite-time stability from [48], the parameters z_{1i}, z_{2i} are chosen to make the function $\Pi_i(\tilde{\theta}_i)$ and its time derivative continuous.

IV. RESULTS AND DISCUSSION

This section presents the experimental results of the position tracking control and force reflecting control with AFOB on the bilateral teleoperation system, which is separated into two aspects. In the first aspect, the accuracy and effectivity of the proposed AFOB scheme for obtaining the external force of the APAM system are compared with multiple state-of-the-art force observers. In the second aspect, to illustrate the

effectiveness of the proposed control scheme in a good transparency performance of both force feedback and position tracking, two typical working sub-scenarios as following:

1) *Free space*: In this working condition, the master and slave robots freely move without the external torques from the human and environment. This test is to verify the effectiveness of the position tracking control scheme. A chirp signal with different amplitudes is chosen as a reference trajectory for the master system to verify the tracking ability of the slave robot. The control algorithm in the master system much drives the master robot to follow the desired trajectory. Moreover, the response of the master side becomes the reference signal of the slave side and the slave controller is developed to make the slave manipulator track the master robot's trajectory. Thus, the effectiveness of the bilateral control scheme is demonstrated by the tracking accuracy of the slave robot position following the desired trajectory given in the master side.
2) *Contact and recovery*: In this working condition, human torque is applied to drive the master robot. Meanwhile, the slave robot will follow the generated trajectory in the master side and contact with the environment. This test is employed to show the transparency performance of the designed teleoperation system. In detail, this experiment process is continuously conducted with free-motion stage and contact motion stage, in an interaction with a ''soft'' environment (low stiffness of the spring is 500 N/mm and damping coefficient of the damper is 4 Ns/mm), and then in an interaction with a ''stiff'' environment (high stiffness of the spring is 2800 N/mm and damping coefficient of the damper is 20 Ns/mm).

In order to validate the genuine perspective on the efficiency of the proposed methods, the experimental testbench is established in Fig. 3. The bilateral teleoperation system consists of two similar manipulators, a control stick for interaction with a human operator, and an environment test bench modeled by an adjustable spring structure and a damper. Each manipulator is actuated by a pair of PAMs (MAS-10-200N-AA-MC-O by Festo company) antagonistically connected through a pulley of radius 0.025 m. The length of each PAM at rest is 0.2 m. The control pressures of both master and slave systems are achieved by two proportional pressure regulator valves (VPPM-8L-L-1-G14-0L8HV1N by Festo company). To obtain the joint position of the manipulators, two optical rotary encoders (E40H12-1024-3-V-5 by Autonis company) with a resolution of 1024 pulse/rev are mounted on the joint structures. Besides, pressure sensors integrated inside the pressure regulators are utilized to obtain the pressure information of the PAMs. The human interacting torque is measured by a torque sensor (Bongshin CDFSA) in the master system. Meanwhile, the interaction force of the slave manipulator with the environment is determined by a force sensor, which is installed in the environment unit. The

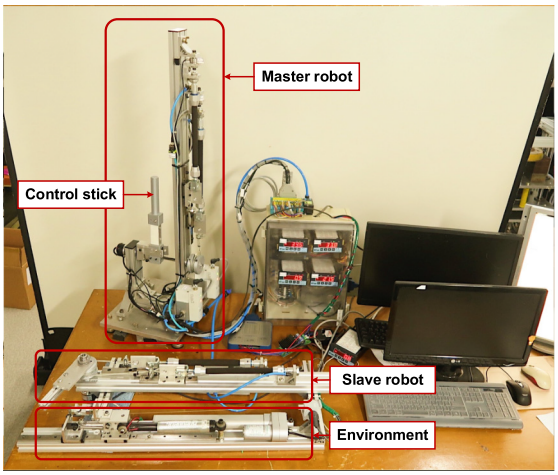

FIGURE 3. Photograph of the experimental appatatus.

TABLE 2. Specifications of the experimental devices.

Device	Description
PAM	Type: Festo MAS-10-200N-AA-MC-O Nominal length: 200 mm Inside diameter: 10 mm Max pressure: 8 bar
PPR Valve	Type: Festo VPPM-8L-L-1-G14-0L8H-V1N Max pressure: 8 bar
DAQ Card	ADVANTECH PCI-1711 AI/AO: 12 bits (resolution) MEASUREMENT PCI-QUAD04
Loadcell	Model: CDFSA Rated capacity: 100 kg Rated output: 1.0 mV/V
Rotary encoder	Type: E40H12-1024-3-V-5 Resolution: 1024 pulses

specifications of the testing devices are shown in Table 2. The overall experiment validation section is evaluated the effectiveness of the proposed control algorithm in the real test bench based on a real-time Windows target toolbox on the MATLAB-Simulink environment. The sampling time t of the real-time process is chosen to be 0.005 second. The disturbance and modeling error are set as $\varepsilon_s = \varepsilon_m = 0.05$. The impendence parameters are selected as $M_d = 1.5$ kg, $B_d = 0.25$ N.s.mm^{-1}, $K_d = 1$ N.mm^{-1}.

A. FORCE ESTIMATION

Three force observers are implemented to obtain the external force from the environment and from the human operator, which are the NDO used in [33], the reaction torque observer (RTOB) with Kalman filter used in [35], and the proposed AFOB. In the NDO design, the force observer gain for the master and the slave system are chosen as $L_h = L_e = 10$. In the RTOB design, the cut-off frequency of the force observer is designed as $\beta = 350$ rad/s. Meanwhile, the parameter configurations of the proposed AFOB are designed as follows $\kappa_i(0) = 0.1$, $\lambda_i = 10$, $\eta_i = 0$, $m = 0.1$, $a = 10$. The torque estimation performances of the three comparative observers in the interaction condition are

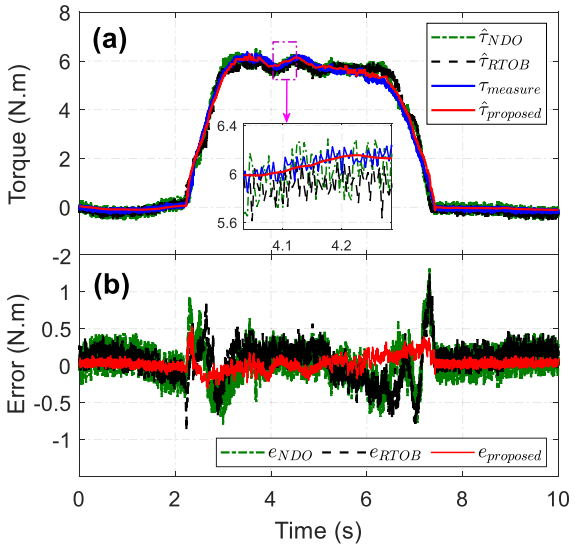

FIGURE 4. Torque estimation performances of the comparative observers in the interaction condition.

depicted in Fig. 4. As shown in Fig. 4 (a), all three observers can fairly obtain the force information with acceptable estimation errors. As described in Fig. 4 (b), however, root-mean-square-errors (RMSEs) associated with NDO, RTOB and proposed algorithm scheme are calculated of 0.211, 0.192 and 0.076, respectively. These results show that the performance of the proposed AFOB is much improved with the smallest steady-state estimation errors and effective noise suppression. With appropriate low-pass filters, the proposed approach shows the robustness with one tuning parameter that needs to be selected but can also achieve high performance. Therefore, this force estimation information can be employed in the force feedback control scheme.

B. TRACKING CONTROL PERFORMANCE

Following the above remarks, assumptions and on the system characteristics in the related study [22], the parameters of the proposed FNTSMC for the master and slave systems are selected as $\lambda_m = \lambda_s = 8$, $p_m = p_s = 5$, $q_m = q_s = 7$, $\varsigma_m = \varsigma_s = 10^{-4}$, $\nu_m = \nu_s = 9/11$, $\varepsilon_m = \varepsilon_s = 0.1$, $\rho_{1m} = \rho_{1s} = 10$, $\rho_{2m} = \rho_{2s} = 2$. Hence, the parameters of the PID controller were initialized by using Zigler-Nichol method, which were selected as $K_P = 3.8$, $K_I = 25$ and $K_D = 0.15$. Based on these parameters, it is considered the basic control gains to provided a suitable control input to compel the system trajectory to its reference as closely as possible. Then, taking advantage of the TSMC and the proposed controller can adjust more specific parameters, which is given the above mention. To more express fair evaluation, the same working conditions have applied simultaneously. Consequently, the experimental results obtained by applying, in turn, the PID, TSMC, and proposed controller to the testing system are shown in Fig. 5, as well as zoom-in in the graph. From Fig. 6 to Fig. 9 show the experimental results of the proposed method where the position and force responses at

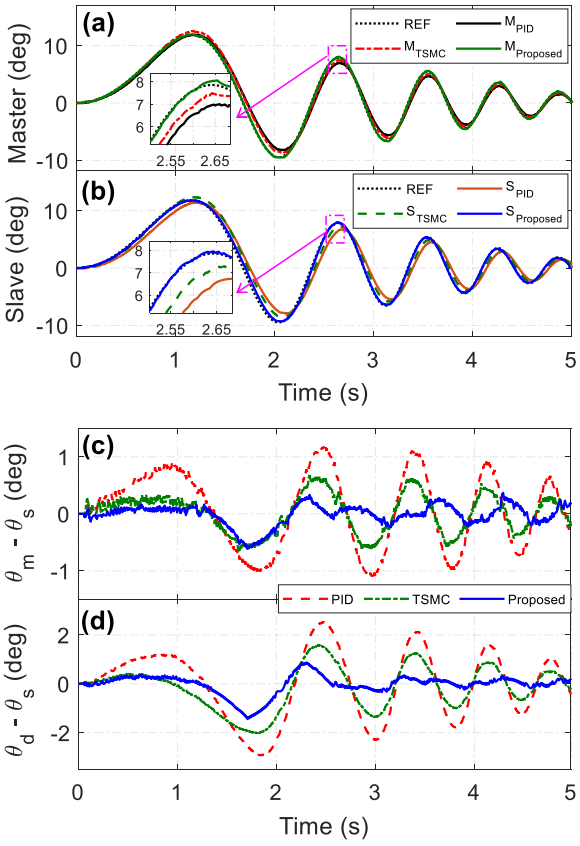

FIGURE 5. Position tracking performances of the comparative control algorithms with respect to the master subsystem.

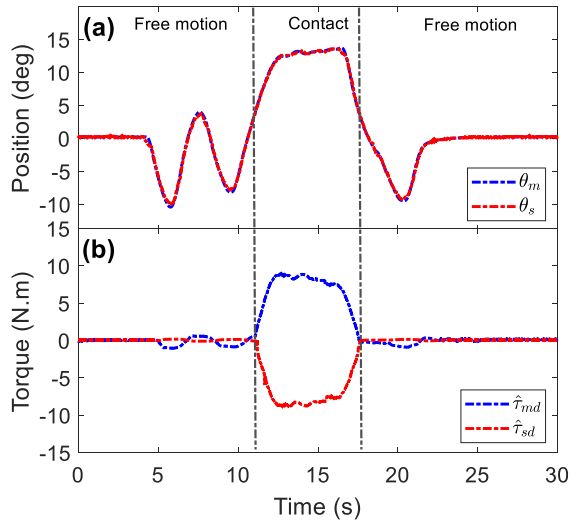

FIGURE 6. Transparency performance of the bilateral teleoperation using haptic control in the free motion and soft contract.

both master and slave sides under various conditions of the environment.

In the free space situation, the desired chirp signal of the frequency of 0.36 Hz with the reducing amplitude by the function $4\pi \times (1 - 0.03t)$ via sampling time t is supplied to the initial command of the master system as seen in Fig. 5.

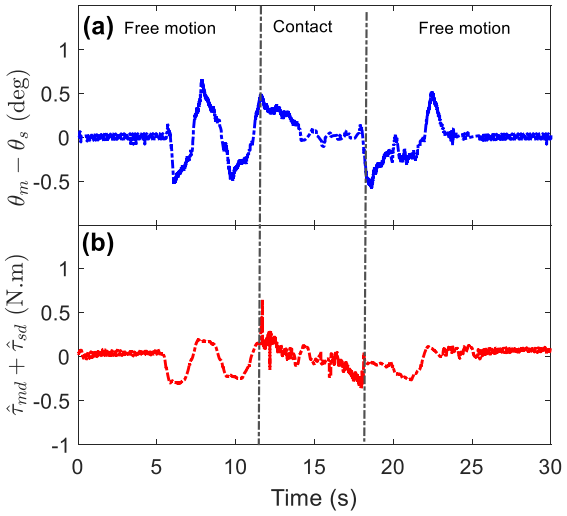

FIGURE 7. Transparency performance of the bilateral teleoperation using haptic control in the free motion and soft contract.

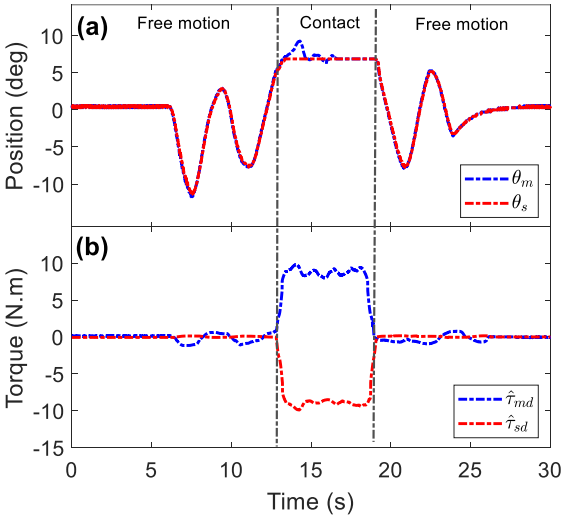

FIGURE 8. Transparency performance of the bilateral teleoperation using haptic control in the free motion and stiff contract.

The output tracking performances of the master and slave are shown in Fig. 5 (a) and (b), as well as zoom-in performance, respectively, whereas Fig. 5 (c) and (d) express the output tracking errors between the master/slave and desired/slave, respectively. For each situation, both master and slave robots are controlled bilaterally with the same pair of PID, TSMC, or proposed controller, respectively. As shown in Fig. 5 (c), the performances of a pair of proposed position control schemes developed by PID framework make acceptable responses of tracking error of ±1.1 deg. Meanwhile, with the TSMC and the proposed controller algorithm improved the control performances with much smaller tracking errors. The tracking errors are mostly limited in an acceptable range of ±0.6 deg, ±0.4 deg, respectively. As results in Fig. 5 (d), it is easily seen that the PID and TSMC performances of the slave robot were significantly degraded with the bound of the tracking error early two times that of

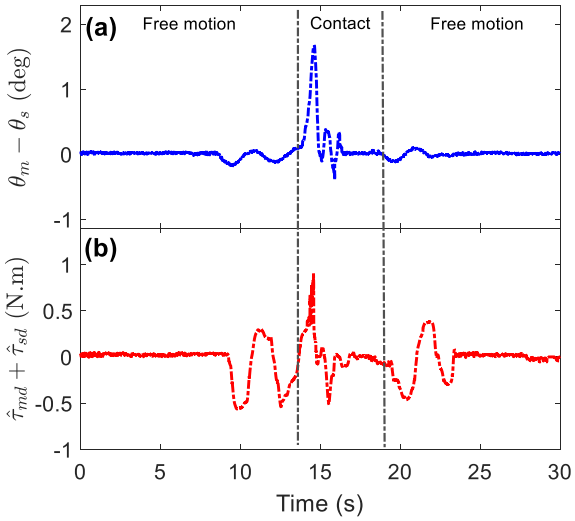

FIGURE 9. Transparency performance of the bilateral teleoperation using haptic control in the free motion and stiff contract.

TABLE 3. Performance indices of comparative controllers.

Controller		PID	TSMC	Proposed
θ_m - θ_s (°)	$L_2[e]$	0.6496	0.3341	0.1823
	e_{max}	1.1178	0.6811	0.3686
θ_d - θ_s (°)	$L_2[e]$	1.4042	0.7053	0.4036
	e_{max}	2.2428	1.5975	0.8394

the performance comparative case of the master/slave robot, from ±1.1 deg to ±2.2 deg, from ±0.6 deg to ±1.3 deg, respectively, whilst the bound of the tracking errors of the proposed controller algorithm is less than 0.8 deg. On the whole, the proposed control method always maintains the great tracking performance between desired command and slave robot within a small range due to its robustness against nonlinearities or uncertainties. In order to have a quantitative comparison between the effectiveness of the control strategies, the tracking errors in Table 3 are calculated by the usage of the integral absolute error ($L_2[e] = \sqrt{(\int_0^T |e|^2\, dt)/T}$), where T is the total experimental time. As shown in this table, the proposed control method is once again confirmed with the smallest tracking errors.

C. TRANSPARENCY PERFORMANCE

In the contact and recovery situation, the initial desired command of the master subsystem is set to a home position, i.e. $\theta_d = 0$. To start with, the environment model is adjusted in low stiffness and damping by the adjusting mechanism. Then the slave manipulator is in a collision with the "soft" environment when $t = 12$ s, and the contact is released when $t = 18$ s as seen in Fig. 6. According to Fig. 6 (a) and Fig. 7 (a), the excellent tracking performance of the slave manipulator following the trajectory from the master manipulator is effectively achieved. As seen in Fig. 6 (b) and Fig. 7 (b), the force transmission in the state of contact is very small in a steady state.

Successively, the environment model is transformed into the ''stiff'' environment with high stiffness and damping as presented in Fig. 8 and Fig. 9. Then the interactions with the environment occur when $t \in [13\text{ s}, 19\text{ s}]$. From these results, there is the overshoot of the master position at the beginning when the interaction of the slave with the environment occurs. However, this overshoot is controllable and the position tracking is also recovered rapidly. It is shown that the tracking performance of the bilateral teleoperation system is still guaranteed despite changing working conditions. Based on the results in Fig. 8 (a) and Fig. 9 (a), the performance of position tracking between the master and the slave is also satisfactory. According to the subfigures *b* in Figs. 8 and Fig. 9, when the system has occurred contact, the error between $\hat{\tau}_{md}$ and $-\hat{\tau}_{sd}$ is also realized.

In short, this also can prove the excellent tracking performances of both master and slave position tracking control scheme in the presence of nonlinearities and uncertainties in the APAM systems. Furthermore, the force reproduces at the master side sensed is in the opposite direction with respect to the force sensed at the slave side, and their sum is small in a steady state. Therefore, the great transparency performance and globally stable of the bilateral haptic teleoperation under the proposed control scheme are achieved despite the uncertainties and in different working conditions.

V. CONCLUSION

This paper proposed a novel force reflecting control approach based on a new adaptive force observer scheme and robust bilateral control for the designed APAM based haptic system under uncertainties. The AFOB approach is designed to obtain the interaction force with an environment for the force reflecting control design with the elimination of the uncertainties and also the noise effect in the obtained force sensing. Then, a robust bilateral control scheme is developed with the combination of the separately fast finite time nonsingular terminal sliding mode control schemes with the force estimation in both subsystems.

Comparative experimental results show that the proposed force observer can obtain accurate force information with noise elimination. This force information is employed in the force reflecting control scheme to improve transparency performance. Finally, the experimental results of the proposed bilateral control in different working conditions show that the provided stability of the overall system and the transparency performance can be attained simultaneously. In the future, we will upgrade the teleoperation test bench with a higher degree of freedom manipulator to extend the application of the teleoperation system.

APPENDIX A

PROOF OF LEMMA 1

For the boundedness of ϑ, a candidate Lyapunov function is selected as follow:

$$V_1 = 0.5\vartheta^T\vartheta \tag{37}$$

Then the time derivative of V_1 is given as

$$\begin{aligned}\dot{V}_1 &= -\vartheta^T\frac{1}{a}\left(\vartheta + \bar{M}_i^{-1}\bar{\Delta}_i + m\sigma_i^*\dot{\tau}_{id}\right)\\ &\le -\frac{1}{m}\vartheta^T\vartheta + \frac{1}{m}\|\vartheta\|\left\|\bar{M}_i^{-1}\bar{\Delta}_i + m\sigma_i^*\dot{\tau}_{id}\right\|\\ &\le -\frac{1}{m}\vartheta^T\vartheta + \frac{1}{2m}\vartheta^T\vartheta + \frac{1}{2m}\left(\bar{M}_i^{-1}\bar{\Delta}_i + m\sigma_i^*\dot{\tau}_{id}\right)^2\\ &\le -\frac{1}{m}V_1 + \frac{1}{2m}\Xi^2\end{aligned} \tag{38}$$

where $\left\|\bar{M}_i^{-1}\bar{\Delta}_i + m\sigma_i^*\dot{\tau}_{id}\right\| \le \Xi$, a Young's inequality is applied to $\|\vartheta\|\left\|\bar{M}_i^{-1}\bar{\Delta}_i + m\sigma_i^*\dot{\tau}_{id}\right\|$. Since $\dot{\tau}_{id}$, σ_i^* and $\bar{\Delta}_i$ are bounded, $\left(\bar{M}_i^{-1}\bar{\Delta}_i + m\sigma_i^*\dot{\tau}_{id}\right)$ is bounded. From the comparison lemma in [46] raised as follows:

$$V_1 \le e^{-t/m}V_1(0) + \frac{1}{2}\Xi^2 \tag{39}$$

Thus, ϑ will exponentially converge to a small compact set bounded by $\|\vartheta(t)\| \le \sqrt{2V_1} \le \Xi$, where its size is determined by the filter parameter m and the upper bound of $\left\|\bar{M}_i^{-1}\bar{\Delta}_i + m\sigma_i^*\dot{\tau}_{id}\right\|$. We can be obtained

$$\lim_{t\to\infty}\|\vartheta(t)\| = \Xi \tag{40}$$

which disappear for sufficiently small m, constant τ_{id} and $\bar{\Delta}_i = 0$. Additionally, $\lim_{t\to 0}\left[\lim_{t\to\infty}\|\vartheta(t)\|\right] = 0$, which means that $\vartheta(t)$ converges to zero for any bounded $\vartheta(0)$ and thus $\vartheta(t) = 0$ is an invariant manifold for $m \to 0$.

APPENDIX B

PROOF OF LEMMA 2

Taking integral of the variables in (15), we have

$$\begin{aligned}\Upsilon_1 &= \int_0^t e^{-a(t-\tau)}\sigma_i^{*T}(\tau)\,\sigma_i^*(\tau)\,d\tau\\ \Upsilon_2 &= \int_0^t e^{-a(t-\tau)}\sigma_i^{*T}\sigma_i^{*T}(\tau)\left(\frac{x_{2i}-x_{2i}^*}{a} - \Lambda_i^*\right)(\tau)\,d\tau\end{aligned} \tag{41}$$

Then, substituting (41) into adaptive law (16) and combining (12). Therefore, we obtain the inequality as following

$$\begin{aligned}\|\Omega\| &\le \int_0^t e^{-a(t-\tau)}\left\|\sigma_i^*\right\|\left(\left\|\sigma_i^*\right\|(\tau_{id}(t) - \tau_{id}(\tau)) + \|\psi(\tau)\|\right)d\tau\\ &\le \int_0^t \left(2\mu_\sigma^2\varepsilon_{\tau_i} + \mu_\sigma\bar{\psi}\right)e^{-a(t-\tau)}d\tau\\ &\le \frac{1}{a}\left(2\mu_\sigma^2\varepsilon_{\tau_i} + \mu_\sigma\bar{\psi}\right).\end{aligned} \tag{42}$$

The proof of the boundedness of Ω is completed.

APPENDIX C

FORCE ESTIMATION

In order to prove the Theorem 1, a Lyapunov candidate function is selected as follows:

$$V_2 = 0.5\delta^{-1}\tilde{\tau}_{id}^T\kappa^{-1}\tilde{\tau}_{id} \tag{43}$$

Taking derivative is calculated along (16) and (17) as

$$\begin{aligned}\dot{V}_2 &= \delta^{-1}\tilde{\tau}_{id}^T\kappa^{-1}\dot{\tilde{\tau}}_{id} + 0.5\delta^{-1}\tilde{\tau}_{id}^T\dot{\kappa}^{-1}\tilde{\tau}_{id} \\ &= \delta^{-1}\tilde{\tau}_{id}^T\kappa^{-1}\left(\dot{\tilde{\tau}}_{id} + \delta\kappa\left[-\Upsilon_1\tilde{\tau}_{id} + \Omega - \eta\sigma_i^{*T}\sigma_i^*\tilde{\tau}_{id}\right.\right. \\ &\quad \left.\left. + \eta\sigma_i^*\psi\right]\right) + 0.5\delta^{-1}\tilde{\tau}_{id}^T\left(-a\kappa^{-1} + \sigma_i^{*T}\sigma_i^*\right)\tilde{\tau}_{id} \\ &\le -\left(e^{-aT}\beta + \frac{ae^{-aT}\beta - \mu_{\sigma_i^*}^2}{2\|\delta\|} - \frac{3}{2\omega}\right)\|\tilde{\tau}_{id}\|^2 \\ &\quad + 0.5\omega\left[\left(\mu_\sigma\bar{\psi}\beta\right)^2 + \frac{\mu_{\tau_{id}}^2}{\|\delta\|^2}\left(\lambda_{\min}(\kappa_0) + \mu_\sigma^2/a\right)^2\right. \\ &\quad \left. + \frac{1}{a^2}\left(2\mu_\sigma^2\varepsilon_{\tau_{id}} + \mu_\sigma\bar{\psi}\right)^2\right] \\ &\le -\eta_{V_2}V_2 + \delta_{V2} \end{aligned} \tag{44}$$

where

$$\begin{aligned}\eta_{V_2} &= \frac{2\|\delta\|}{\lambda_{\min}(\kappa_0) + \mu_\sigma^2/a} \\ &\quad \times \left(e^{-aT}\beta + \frac{ae^{-aT}\beta - \mu_\sigma^2}{2\|\delta\|} - \frac{3}{2\omega}\right)\|\tilde{\tau}_{id}\|^2 \\ \delta_{V_2} &= 0.5\omega\left[\left(\mu_\sigma\bar{\psi}\beta\right)^2 + \frac{\mu_{\tau_{id}}^2}{\|\delta\|^2}\left(\lambda_{\min}(\kappa_0) + \mu_\sigma^2/a\right)^2\right. \\ &\quad \left. + \frac{1}{a^2}\left(2\mu_\sigma^2\varepsilon_{\tau_{id}} + \mu_\sigma\bar{\psi}\right)^2\right] \\ \left\|\dot{\tilde{\tau}}_{id}\right\| &\le \mu_{\tau_{id}}\end{aligned}$$

and ω is a positive constant scalar. Based on [46], from the inequality (44)

$$V_2(t) \le e^{-\eta_{V_2}t}V_2(0) + \frac{\delta_{V_2}}{\eta_{V_2}}. \tag{45}$$

Therefore, the external force estimation errors converge to the compact set defined as follows

$$\|\tilde{\tau}_{id}\| \le \sqrt{\frac{2\|\delta\|\,\delta_{V_2}\beta}{\eta_{V_2}e^{aT}}} = \bar{\zeta}_i \tag{46}$$

APPENDIX D
MASTER CONTROLLER

For the master system, a Lyapunov candidate function is selected to proof the Theorem 2 as

$$V_3(t) = 0.5s_m^T\bar{M}_m s_m \tag{47}$$

Using the derivative of the sliding surface (24), the time derivative of $V_3(t)$ can be written as

$$\begin{aligned}\dot{V}_3 &= s_m^T\bar{M}_m\dot{s}_m + 0.5s_m^T\dot{\bar{M}}_m s_m \\ &= s_m\left[-\bar{M}_m\ddot{\tilde{\theta}}_{mr} - \bar{C}_m\dot{\tilde{\theta}}_{mr} - \bar{K}_m\theta_m + \tau_m - \tau_{md} - \bar{C}_m s_m\right] \\ &\quad + 0.5s_m^T\dot{\bar{M}}_m s_m \\ &\le s_m\left[\varepsilon_m sign(s_m) - \rho_{1m}s_m - \rho_{2m}s_m^{[v_m]} + \hat{\tau}_{md} - \tau_{md}\right] \\ &\quad + 0.5s_m^T\left[\dot{\bar{M}}_m - 2\bar{C}_m\right]s_m \\ &\le -\varepsilon_m|s_m| - \rho_{1m}s_m^2 - \rho_{2m}s_m^{[v_m+1]} + s_m\left(\hat{\tau}_{md} - \tau_{md}\right) \\ &\le -\rho_{1m}s_m^2 - \rho_{2m}s_m^{[v_m+1]} = -2\rho_{1m}V_3 - 2\rho_{2m}V_3^{[v_m+1]/2} \end{aligned} \tag{48}$$

According to the finite time stability from [47] and [48], the variable sliding surfaces can converge to zero in finite time can converge to zero in a finite time. Then the tracking error $\tilde{\theta}_m$can reach zero in a finite time.

The proof of Theorem 2 is completed.

APPENDIX E
SLAVE CONTROLLER

In order to demonstrate the Theorem 3, a Lyapunov candidate function is selected as

$$V_4(t) = 0.5s_s^T\bar{M}_s s_s \tag{49}$$

Using the derivative of the sliding surface (29), the time derivative of $V_4(t)$ can be written as

$$\begin{aligned}\dot{V}_4 &= s_s^T\bar{M}_s\dot{s}_s + 0.5s_s^T\dot{\bar{M}}_s s_s \\ &= s_s\left[-\bar{M}_s\ddot{\tilde{\theta}}_{sr} - \bar{C}_s\dot{\tilde{\theta}}_{sr} - \bar{K}_s\theta_s + \tau_s - \tau_{sd} - \bar{C}_s s_s\right] \\ &\quad + 0.5s_s^T\dot{\bar{M}}_s s_s \\ &= s_s\left[\varepsilon_s sign(s_s) - \rho_{1s}s_s - \rho_{2s}s_s^{[v_s]} + \hat{\tau}_{sd} - \tau_{sd}\right] \\ &\quad + 0.5s_s^T\left[\dot{\bar{M}}_s - 2\bar{C}_s\right]s_s \\ &= -\varepsilon_s|s_s| - \rho_{1s}s_s^2 - \rho_{2s}s_s^{[v_s+1]} + s_s\left(\hat{\tau}_{sd} - \tau_{sd}\right) \\ &\le -\rho_{1s}s_s^2 - \rho_{2s}s_s^{[v_s+1]} = -2\rho_{1s}V_4 - 2\rho_{2s}V_4^{[v_s+1]/2} \end{aligned} \tag{50}$$

For the finite-time stability from [47] and [48], the variable sliding surfaces can converge to zero in finite time can converge to zero in a finite time. Then the tracking error $\tilde{\theta}_s$ can reach zero in a finite time.

The proof of Theorem 3 is completed.

REFERENCES

[1] D. Wang, K. Ohnishi, and W. Xu, "Novel emerging sensing, actuation, and control techniques for haptic interaction and teleoperation," *IEEE Trans. Ind. Electron.*, vol. 67, no. 1, pp. 624–626, Jan. 2020.

[2] D. Q. Truong, B. N. M. Truong, N. T. Trung, S. A. Nahian, and K. K. Ahn, "Force reflecting joystick control for applications to bilateral teleoperation in construction machinery," *Int. J. Precis. Eng. Manuf.*, vol. 18, no. 3, pp. 301–315, Mar. 2017.

[3] H. Li, K. Kawashima, K. Tadano, S. Ganguly, and S. Nakano, "Achieving haptic perception in Forceps' manipulator using pneumatic artificial muscle," *IEEE/ASME Trans. Mechatronics*, vol. 18, no. 1, pp. 74–85, Feb. 2013.

[4] J. Aleotti, G. Micconi, S. Caselli, G. Benassi, N. Zambelli, M. Bettelli, and A. Zappettini, "Detection of nuclear sources by UAV teleoperation using a visuo-haptic augmented reality interface," *Sensors*, vol. 17, no. 10, p. 2234, Sep. 2017.

[5] Y. Wang, L. Gu, Y. Xu, and X. Cao, "Practical tracking control of robot manipulators with continuous fractional-order nonsingular terminal sliding mode," *IEEE Trans. Ind. Electron.*, vol. 63, no. 10, pp. 6194–6204, Oct. 2016.

[6] T. D. C. Thanh and K. K. Ahn, "Nonlinear PID control to improve the control performance of 2 axes pneumatic artificial muscle manipulator using neural network," *Mechatronics*, vol. 16, no. 9, pp. 577–587, Nov. 2006.

[7] J. Park and O. Khatib, "A haptic teleoperation approach based on contact force control," *Int. J. Robot. Res.*, vol. 25, nos. 5–6, pp. 575–591, May 2006.
[8] U. J. Na and M. Hung Vu, "Adaptive impedance control of a haptic teleoperation system for improved transparency," in *Proc. IEEE Int. Workshop Haptic Audio Vis. Environ. Games (HAVE)*, Oct. 2012, pp. 38–43.
[9] K. Kawashima, T. Sasaki, A. Ohkubo, T. Miyata, and T. Kagawa, "Application of robot arm using fiber knitted type pneumatic artificial rubber muscles," in *Proc. IEEE Int. Conf. Robot. Autom. ICRA*, Apr. 2004, pp. 4937–4942.
[10] T. D. C. Thanh and K. K. Ahn, "Intelligent phase plane switching control of pneumatic artificial muscle manipulators with magneto-rheological brake," *Mechatronics*, vol. 16, no. 2, pp. 85–95, Mar. 2006.
[11] N. Wang, J.-C. Sun, and M. J. Er, "Tracking-error-based universal adaptive fuzzy control for output tracking of nonlinear systems with completely unknown dynamics," *IEEE Trans. Fuzzy Syst.*, vol. 26, no. 2, pp. 869–883, Apr. 2018.
[12] J. Fei, Y. Chu, and S. Hou, "A backstepping neural global sliding mode control using fuzzy approximator for three-phase active power filter," *IEEE Access*, vol. 5, pp. 16021–16032, 2017.
[13] X. Ma, F. Sun, H. Li, and B. He, "Neural-network-based integral sliding-mode tracking control of second-order multi-agent systems with unmatched disturbances and completely unknown dynamics," *Int. J. Control, Autom. Syst.*, vol. 15, no. 4, pp. 1925–1935, Aug. 2017.
[14] Y. Wang, L. Liu, D. Wang, F. Ju, and B. Chen, "Time-delay control using a novel nonlinear adaptive law for accurate trajectory tracking of cable-driven robots," *IEEE Trans. Ind. Informat.*, vol. 16, no. 8, pp. 5234–5243, Aug. 2020.
[15] Y. Wang, F. Yan, K. Zhu, B. Chen, and H. Wu, "A new practical robust control of cable-driven manipulators using time-delay estimation," *Int. J. Robust Nonlinear Control*, vol. 29, no. 11, pp. 3405–3425, Jul. 2019.
[16] T. X. Dinh and K. K. Ahn, "Radial basis function neural network based adaptive fast nonsingular terminal sliding mode controller for piezo positioning stage," *Int. J. Control, Autom. Syst.*, vol. 15, no. 6, pp. 2892–2905, Oct. 2017.
[17] H. Aschemann and D. Schindele, "Sliding-mode control of a high-speed linear axis driven by pneumatic muscle actuators," *IEEE Trans. Ind. Electron.*, vol. 55, no. 11, pp. 3855–3864, Nov. 2008.
[18] N. Wang, Z. Sun, Y. Jiao, and G. Han, "Surge-heading guidance-based finite-time path following of underactuated marine vehicles," *IEEE Trans. Veh. Technol.*, vol. 68, no. 9, pp. 8523–8532, Sep. 2019.
[19] L. Qiao and W. Zhang, "Double-loop integral terminal sliding mode tracking control for UUVs with adaptive dynamic compensation of uncertainties and disturbances," *IEEE J. Ocean. Eng.*, vol. 44, no. 1, pp. 29–53, Jan. 2019.
[20] Y. Wang, F. Yan, J. Chen, F. Ju, and B. Chen, "A new adaptive time-delay control scheme for cable-driven manipulators," *IEEE Trans. Ind. Informat.*, vol. 15, no. 6, pp. 3469–3481, Jun. 2019.
[21] N. Wang and C. K. Ahn, "Hyperbolic-tangent LOS guidance-based finite-time path following of underactuated marine vehicles," *IEEE Trans. Ind. Electron.*, early access, Oct. 22, 2019, doi: 10.1109/TIE.2019.2947845.
[22] C. P. Vo, X. D. To, and K. K. Ahn, "A novel adaptive gain integral terminal sliding mode control scheme of a pneumatic artificial muscle system with time-delay estimation," *IEEE Access*, pp. 2169–3536, 2019.
[23] N. Wang and H. He, "Dynamics-level finite-time fuzzy monocular visual servo of an unmanned surface vehicle," *IEEE Trans. Ind. Electron.*, early access, Nov. 15, 2020, doi: 10.1109/TIE.2019.2952786.
[24] Y. Wang, K. Zhu, B. Chen, and M. Jin, "Model-free continuous nonsingular fast terminal sliding mode control for cable-driven manipulators," *ISA Trans.*, vol. 98, pp. 483–495, Mar. 2020.
[25] L. Qiao and W. Zhang, "Trajectory tracking control of AUVs via adaptive fast nonsingular integral terminal sliding mode control," *IEEE Trans. Ind. Informat.*, vol. 16, no. 2, pp. 1248–1258, Feb. 2020.
[26] Z. Chen, F. Huang, C. Yang, and B. Yao, "Adaptive fuzzy backstepping control for stable nonlinear bilateral teleoperation manipulators with enhanced transparency performance," *IEEE Trans. Ind. Electron.*, vol. 67, no. 1, pp. 746–756, Jan. 2020.
[27] Y. Yuan, Y. Wang, and L. Guo, "Force reflecting control for bilateral teleoperation system under time-varying delays," *IEEE Trans. Ind. Informat.*, vol. 15, no. 2, pp. 1162–1172, Feb. 2019.
[28] F. Huang, W. Zhang, Z. Chen, J. Tang, W. Song, and S. Zhu, "RBFNN-based adaptive sliding mode control design for nonlinear bilateral teleoperation system under time-varying delays," *IEEE Access*, vol. 7, pp. 11905–11912, 2019.
[29] F. Zeng, J. Xiao, and H. Liu, "Force/Torque sensorless compliant control strategy for assembly tasks using a 6-DOF collaborative robot," *IEEE Access*, vol. 7, pp. 108795–108805, 2019.
[30] F. Zhou, B. Dong, and Y. Li, "Torque sensorless force/position decentralized control for constrained reconfigurable manipulator with harmonic drive transmission," *Int. J. Control, Autom. Syst.*, vol. 15, no. 5, pp. 2364–2375, Sep. 2017.
[31] N. Wang and Z. Deng, "Finite-time fault estimator based fault-tolerance control for a surface vehicle with input saturations," *IEEE Trans. Ind. Informat.*, vol. 16, no. 2, pp. 1172–1181, Feb. 2020.
[32] T. Q. Dinh, J. I. Yoon, J. Marco, P. Jennings, K. K. Ahn, and C. Ha, "Sensorless force feedback joystick control for teleoperation of construction equipment," *Int. J. Precis. Eng. Manuf.*, vol. 18, no. 7, pp. 955–969, Jul. 2017.
[33] H. Amini, B. Farzaneh, F. Azimifar, and A. A. D. Sarhan, "Sensor-less force-reflecting macro–micro telemanipulation systems by piezoelectric actuators," *ISA Trans.*, vol. 64, pp. 293–302, Sep. 2016.
[34] L. Chan, F. Naghdy, and D. Stirling, "An improved extended active observer for adaptive control of a *n*–DOF robot manipulator," *J. Intell. Robotic Syst.*, vol. 85, nos. 3–4, pp. 679–692, Jul. 2016.
[35] C. Mitsantisuk, K. Ohishi, and S. Katsura, "Estimation of action/reaction forces for the bilateral control using Kalman filter," *IEEE Trans. Ind. Electron.*, vol. 59, no. 11, pp. 4383–4393, Nov. 2012.
[36] T. T. Phuong, K. Ohishi, and Y. Yokokura, "Fine sensorless force control realization based on dither periodic component elimination Kalman filter and wide band disturbance observer," *IEEE Trans. Ind. Electron.*, vol. 67, no. 1, pp. 757–767, Jan. 2020.
[37] C.-P. Chou and B. Hannaford, "Measurement and modeling of McKibben pneumatic artificial muscles," *IEEE Trans. Robot. Autom.*, vol. 12, no. 1, pp. 90–102, Feb. 1996.
[38] D. Zhang, X. Zhao, and J. Han, "Active model-based control for pneumatic artificial muscle," *IEEE Trans. Ind. Electron.*, vol. 64, no. 2, pp. 1686–1695, Feb. 2017.
[39] A. Merola, D. Colacino, C. Cosentino, and F. Amato, "Model-based tracking control design, implementation of embedded digital controller and testing of a biomechatronic device for robotic rehabilitation," *Mechatronics*, vol. 52, pp. 70–77, Jun. 2018.
[40] A. F. Filippov, *Differential Equations With Discontinuous Right-Hand Sides*. Dordrecht, The Netherlands: Kluwer, 1988, pp. 48–122.
[41] R. Kelly, V. S. Davila, and J. A. L. Perez, "Control of robot manipulators in joint space," in *Advanced Textbooks in Control and Signal Processing*. Glasgow, Scotland: Univ. Strathclyde, Mar. 2005, pp. 20–26.
[42] P. A. Ioannou and J. Sun, "On-line parameter estimation," in *Robust Adaptive Control*, Mineola, NY, USA: Dover, 2012, pp. 144–245.
[43] J. Na, G. Herrmann, R. Burke, and C. Brace, "Adaptive input and parameter estimation with application to engine torque estimation," in *Proc. 54th IEEE Conf. Decis. Control (CDC)*, Dec. 2015, pp. 3687–3692.
[44] M. N. Mahyuddin, J. Na, G. Herrmann, X. Ren, and P. Barber, "Adaptive observer-based parameter estimation with application to road gradient and vehicle mass estimation," *IEEE Trans. Ind. Electron.*, vol. 61, no. 6, pp. 2851–2863, Jun. 2014.
[45] S. Sastry and M. Bodson, "Preliminaries," in *Adaptive Control: Stability, Convergence, and Robustness*. Upper Saddle River, NJ, USA: Prentice-Hall, 1989, pp. 17–39.
[46] H. K. Khalil, "Lyapunov stability," in *Nonlinear Systems*, vol. 9, 3rd ed. Upper Saddle River, NJ, USA: Prentice-Hall, 2002, pp. 111–181.
[47] D. Zhao, S. Li, Q. Zhu, and F. Gao, "Robust adaptive terminal sliding mode-based synchronised position control for multiple motion axes systems," *IET Control Theory Appl.*, vol. 3, no. 1, pp. 136–150, Jan. 2009.
[48] T. X. Dinh and K. K. Ahn, "Adaptive-gain fast nonsingular terminal sliding mode for position control of a piezo positioning stage," *Proc. Inst. Mech. Eng., I, J. Syst. Control Eng.*, vol. 232, no. 8, pp. 994–1014, May 2018.

CONG PHAT VO received the B.E. degree in electrical and electronic engineering technology and the M.Sc. degree in mechatronics engineering from the Ho Chi Minh City University of Technology and Education, Vietnam, in 2013 and 2016, respectively. He is currently pursuing the Ph.D. degree with the School of Mechanical Engineering, University of Ulsan, Ulsan, South Korea.

His research interests include nonlinear control, smart actuator/materials, and renewable energy.

XUAN DINH TO received the B.S. degree from the Department of Mechanical Engineering, Le Quy Don Technical University, Hanoi, Vietnam, in 2012.

He is currently a Postdoctoral Researcher with the School of Mechanical Engineering, University of Ulsan, Ulsan, South Korea, and also a Researcher with the Faculty of Control Engineering, Le Quy Don Technical University. His research interests include robotics, smart actuators/materials, and nonlinear control.

KYOUNG KWAN AHN (Senior Member, IEEE) received the B.S. degree from the Department of Mechanical Engineering, Seoul National University, in 1990, the M.Sc. degree in mechanical engineering from the Korea Advanced Institute of Science and Technology, in 1992, and the Ph.D. degree from the Tokyo Institute of Technology, in 1999.

He is currently a Professor at the School of Mechanical Engineering, University of Ulsan, Ulsan, South Korea. His research interests are design and control of smart actuator using the smart material, fluid power control and active damping control, and renewable energy. He is an Editor of IJCAS and on the Editorial Board of *Renewable Energy*, *Actuators*, and *Journal of Engineering*.